Hemodynamics and the Vascular Endothelial Cytoskeleton

Ira M. Herman,* Arthur M. Brant,‡ Vijay S. Warty,§ Jan Bonaccorso,* Edwin C. Klein,‖ Robert L. Kormos,‡ and Harvey S. Borovetz‡

*Department of Anatomy and Cellular Biology, Tufts University School of Medicine, Boston, Massachusetts 02111; ‡Departments of Surgery, §Pathology, and ‖Animal Laboratory Resources, University of Pittsburgh School of Medicine, Pittsburgh, Pennsylvania 15261

Abstract. Although there is considerable evidence to suggest that hemodynamics play an important role in vascular disease processes, the exact mechanisms are unknown. With this in mind, we have designed a pulsatile perfusion apparatus which reproducibly delivers pulsatile hemodynamics upon freshly excised canine carotid arteries in vitro. Quantifiable simulations included (a) normotension with normal or lowered flow rates (120/80 mmHg, 120 and 40 ml/min), (b) normotension with lowered or elevated transmural pressures (40–170 mmHg), and (c) elevated pulse pressure (120 and 80 mmHg) with normal (150 ml/min) or elevated rates of flow (300 and 270 ml/min). Arterial biomechanical stresses and cellular behaviors were characterized biochemically and morphologically under all these simulations which continued for 2–24 h. We found that increased pulse pressure alone had little effect on the total amount of radiolabeled [4-^{14}C]cholesterol present within the medial compartment. However, normotension when coupled with altered transmural pressure yielded a three- to fourfold increase.

Combinations of increased pulse pressure and flow potentiated cholesterol uptake by a factor of 10 when compared with normotension control values. Simulations that enhanced carotid arterial cholesterol uptake also influenced the endothelial cytoskeletal array of actin. Stress fibers were not present within the carotid endothelial cells of either the sham controls or the normotension and increased pulse pressure (normal flow) simulations. Endothelial cells lining carotids exposed to elevations in flow or those present within vessels perfused as per simulation b above assembled stress fibers ($x = 4$ and 10 per cell, respectively) within the time course of these studies. When endothelial cells were subjected to hemodynamic conditions that potentiated maximally cholesterol transport, no diffuse or stress fiber staining could be seen, but the cortical array of actin was intact. These results suggest that those biomechanical stresses that alter endothelial permeability and intimal integrity may do so via cytoskeletal actin signaling.

R ECENT experimental evidence indicates that endothelial cells (EC),[1] which line the blood vascular systems of higher vertebrates, are actively involved in maintenance of intimal integrity. This stabilization against the blood shearing forces and biomechanical wall stresses at the luminal–EC interface may be directly related to the intimal cells' ability to synthesize and organize (a) junctional elements, (b) materials of the basal laminae that promote EC adhesion to the extracellular matrix, and (c) an intricate cytoskeleton composed of contractile and structural proteins needed to modulate the luminal–abluminal shear zone.

Early work in vitro revealed that vascular EC possessed linear cytoplasmic fibrils (16). Naming the structures "tension striae," the Lewises proposed that these elements (later renamed "stress fibers") promoted adhesion of cells to the underlying substrate. A structural rather than motile role for stress fibers is consistent with more recent in vitro studies which show an inverse relationship between the rate of cell movement and the number of stress fibers within the cytoplasmic matrix (12, 17). The dynamics of stress fiber assembly has also been examined, but, again their appearance in nonmuscle cytoplasm is highly coincident with slowly moving or immobilized cells (25). Of late, stress fibers have been identified in vascular EC in situ. Their presence has been noted in regions of the arterial vasculature exposed to elevated blood velocities (14, 28), and perhaps, EC stress fiber presence indicates or reflects a unique cellular response to a specific hemodynamic environment. Stress fiber modulation has also been noted during the vascular disease states of hypertension (26), atherogenesis (11), as well as in association with angiogenesis (13). Moreover, extracellular matrix molecules (some of which are present within the basal laminae of blood vessels), have also been shown to induce stress fiber assembly (29). This extracellular signaling of the endothelial cytoskeleton may contribute to vascular disease progression. Indeed, the inability of injured arterial EC to

---

1. *Abbreviations used in this paper*: EC, endothelial cell(s); PDA, pulse duplicator apparatus; SEM, scanning electron microscopy.
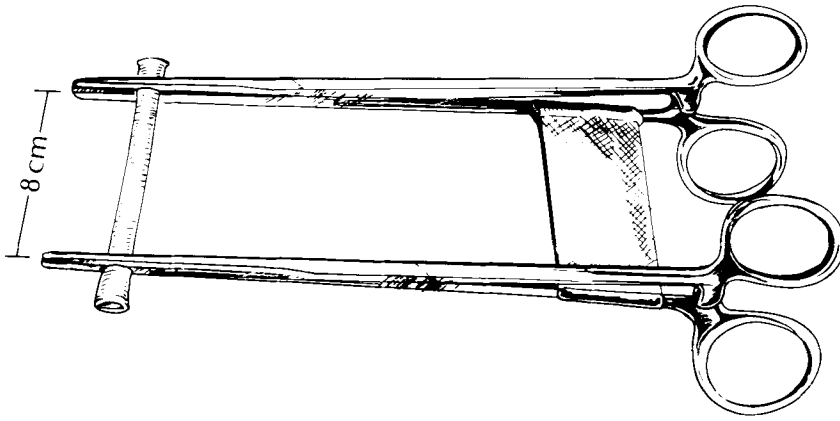
repopulate (via migration) wounded areas of intima in animals may be stress fiber–related.

Because the vascular EC cytoskeleton is believed critical to intimal integrity and has been shown to modulate with hemodynamics and the vascular disease state, we have developed a model system to test, under controlled and repeatable experimental conditions, whether blood flow phenomena induce cytostructural assembly and thereby promote intimal integrity on the one hand, or influence cytoskeletal disruption and intimal destabilization on the other. The pulsatile flow, pulse duplicator apparatus (PDA), when fitted to the ca-

nine carotid artery, provides important new data regarding the hemodynamic variables that modulate the endothelial cytoskeletal array of actin and, at the same time, promote macromolecular transport across the arterial wall. Our results suggest that when increased rates of pulsatile flow are combined with elevated pulse pressures and nonphysiologic vessel wall motion, there are significant adaptive alterations in EC morphology, actin array, and cholesterol uptake. These subcellular modifications of the carotid intimal layer may contribute to the hemodynamics-induced arterial diseased state.
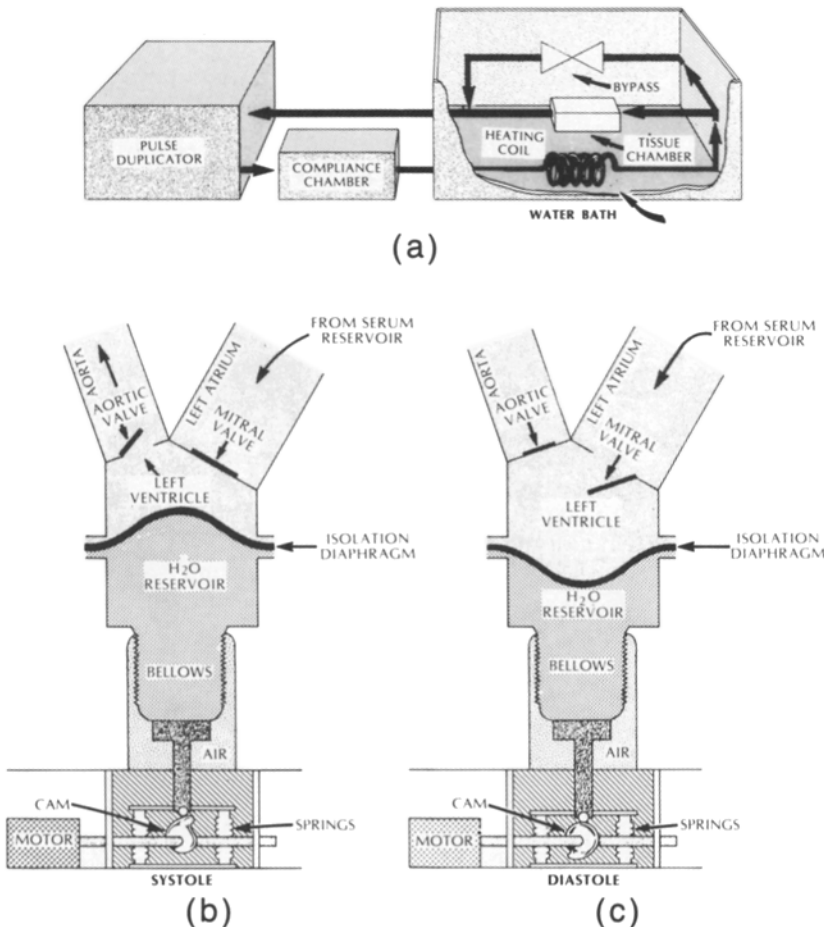

(a)

(b)

(c)

Figure 2. Schematic diagram of pulsatile perfusion apparatus. (*a*) Block diagram and flow path; (*b*) pumping chamber in systole showing mechanical components of the flow delivery system; (*c*) pumping chamber in diastole. A computer-aided designed and manufactured disc cam and roller follower provided the pulsatile pressure and flow waveforms that simulated the vascular hemodynamic environment (1).
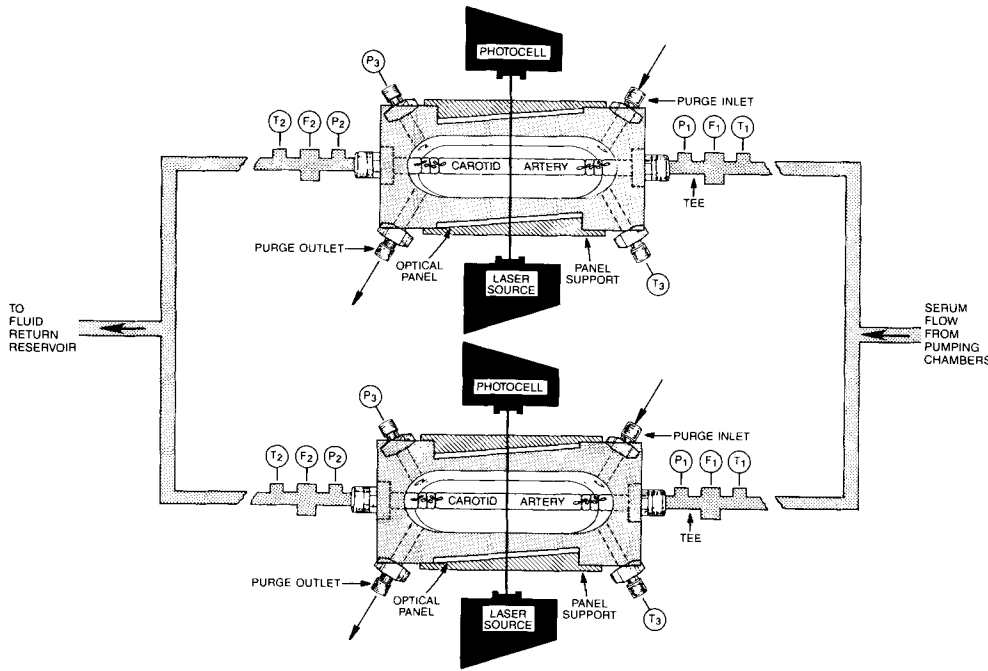
Figure 3. Tissue housing chambers showing simultaneous perfusion of two excised carotids and sites of in vitro measurement. Abbreviations: P, pressure; F, flow rate; T, temperature; 1, proximal; 2, distal; 3, adventitial. The excised carotids were secured in the tissue housing chamber using suture material.

Materials and Methods

Animal Model

Only dogs intended for sacrifice served as the vessel donors. All animals were anesthetized with sodium pentobarbital (30 mg/kg) before we made a ventral midline neck incision. One common carotid artery was carefully exposed and all visible vessels associated with the artery were ligated. To avoid EC damage (owing to vessel collapse), the in vivo length and diameter of the carotid arteries were maintained during and after surgical excision and throughout each perfusion study (Fig. 1). Vessel orientation was marked with india ink to insure the correct (in vivo) perfusion direction. Removal of the second carotid artery began 30 min after the first carotid was secured in the PDA. Thus, a single animal served to provide an experimental and a control vessel segment for simultaneous pulsatile perfusion (e.g., normotension vs. increased pulse pressure). All animal procedures were performed in accordance with National Institutes of Health and University of Pittsburgh guidelines for the care and use of laboratory animals.

PDA

In vitro experiments were performed using the pulsatile perfusion apparatus (Fig. 2) described by Brant et al. (1). Excised canine carotid arteries were secured in the tissue housing chambers of the perfusion apparatus (Fig. 3), which contained the associated instrumentation to allow for nine dynamic measurements during pulsatile perfusion including the monitoring of the proximal and distal perfusion pressures, flow rates and temperatures, pressure and temperature within the fluid bathing the adventitia of the perfused carotids, and the pulsating outer diameter of the canine carotids. The latter were determined in a noncontacting fashion using a scanning laser micrometer (2). Sites of measurements are shown schematically in Fig. 3. As described previously (1–3) the perfusate medium employed in all experiments was freshly prepared canine serum. The adventitial bathing fluid was normothermic Ringer's lactate.

Hemodynamic Simulations. Several physiologic/pathophysiologic vascular hemodynamic simulations were imposed upon the test carotid arteries (Table I). We selected as our "control" a normothermic (37°C) perfusion experiment, which imposed upon a test carotid artery an intralumenal and transmural pressure of 120/80 mmHg, a pulse rate of 1 Hz, and a perfusion rate of 120–150 ml/min. This experimental case is listed in group I of Table I along with a second simulation in which the perfusion rate was reduced to 40 ml/min without affecting the intralumenal or transmural pressures. In group II experiments, the mean transmural pressure was varied (from 100 mmHg) to alter the compliance of the vessel wall. Here we maintained the

proximal perfusion pressure (P_1 in Fig. 3) at 120/80 mmHg and pulse pressure at 40 mmHg while adjusting the pressure in the adventitial bathing fluid to achieve the desired mean transmural pressures. An increase in transmural pressure from 100 to 170 mmHg reduced the magnitude of radial pulsations of the vessel wall and simulated decreased vessel compliance. When the transmural pressure was reduced to 40 mmHg, the opposite effects were noted (3). The importance of pulse pressure and rate of flow upon the EC cytoskeleton was also investigated. In the group III experiments, pulse pressure (PP) was raised from 40 mmHg (groups I and II) to 120 mmHg; the mean perfusion rate was either fixed at the nominal value of 150 ml/min or doubled to 300 ml/min. The final condition in the group III category, hypertension/↑flow, was selected to simulate the clinical situation of hypertension. During all perfusion experiments, care was exercised to maintain the pH, Po_2, and Pco_2 of the serum perfusate within physiologic limits.

Biochemical Procedures

Incorporation of Radiolabel [4-^{14}C] Cholesterol into Serum. To measure the uptake of cholesterol during pulsatile perfusion, labeled cholesterol was added to the freshly prepared canine serum prior to delivery into the PDA circuit. Briefly, [4-^{14}C]-labeled cholesterol (New England Nuclear, Boston, MA; 500 μCi, 59 mCi/mmol) was placed in a closed fume hood, and the benzene solvent was evaporated to dryness under a constant stream of oxygen-free nitrogen at room temperature. The dried labeled cholesterol was then dissolved in 1 ml of 95% ethanol (20). 500 ml of the freshly prepared dog serum was then added to the ethanol-cholesterol mixture and the

Table I. Simulated Hemodynamic Environments

Group	Simulation	Mean transmural pressure	Mean perfusion rate
		mmHg	*ml/min*
I	Normotension	100 (120/80)	120
I	Normotension – ↓flow	100 (110/90)	40
II	Normotension – ↑TP	170 (190/150)	150
II	Normotension – ↓TP	40 (60/20)	150
III	↑PP/↑TP	180 (240/120)	150
III	↑PP/↑TP/↑flow	180 (240/120)	300
III	Hypertension/↑flow	130 (170/90)	270

Abbreviations: PP, pulse pressure; TP, transmural pressure.

Figure 5. Light microscopy demonstration of intimal integrity under normotension, normal flow hemodynamics (group I simulation of Table I). Canine carotid EC were carefully stripped from the intima (sharp dissection) and the cell borders were delineated with a silver nitrate staining method (15). An intact endothelium is present. Bar, 10 μm.
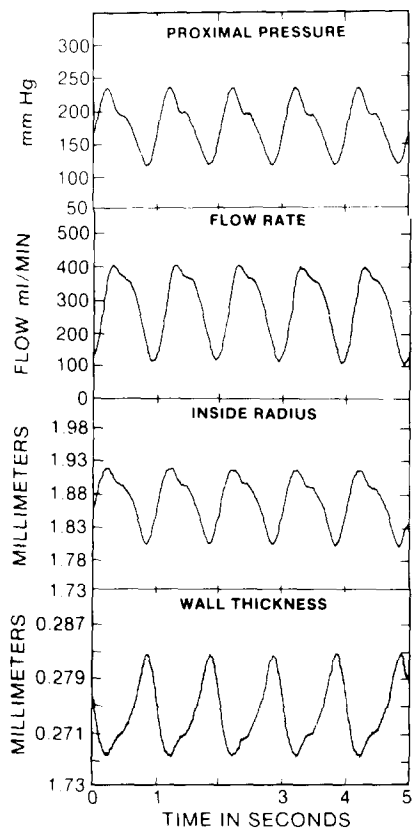
Figure 4. Hemodynamic tracings obtained during one experiment of ↑PP/↑TP/↑flow. The top waveform, proximal pressure, was taken from sensor P_1 of Fig. 3; the flow tracing was measured at F_1. Data of arterial geometry was derived from the laser waveforms described in Brant et al. (2, 3).

entire solution was stirred at 37°C under nitrogen atmosphere for a period of 2 h. Using this procedure between 86% and 92% incorporation is obtained, the radioactivity ranging from 0.86 to 0.92 μCi/ml.

Postperfusion Tissue Processing for EC Localization Studies

Perfusion Fixation of Canine Carotid Segments. Arterial segments (4 cm) were placed immediately after their removal from the PDA in a specially designed perfusion fixation circuit. This circuit consisted of a commercial roller pump, interconnecting sterile polyvinyl chloride tubing, and a single-tissue housing chamber identical to that shown in Fig. 3. The fixative was freshly prepared 4% buffered (pH 7.4) formaldehyde in isotonic saline. After a 20-min normothermic perfusion-fixation at the particular mean pressure of the just-completed experiment, the vessel was tied off while in its distended, in vivo state and shipped in the 4% buffered-formaldehyde to
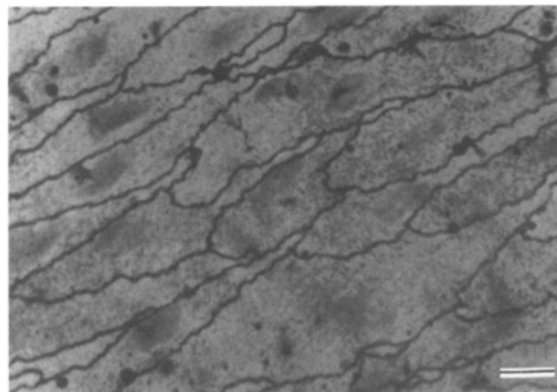
Tufts Medical School by air express. Thus, cytoskeletal localizations of the carotid EC actin were performed within 24 h of fixation. Storage in 4% buffered formaldehyde, however, did not influence the morphology or the localization studies performed.

Localization of Endothelial Cell Actin with Affinity-purified Antibodies and Fluorescence Microscopy. Perfusion-fixed segments of the canine carotids were received in a coded, blind fashion and were washed free of aldehyde in a buffer containing 0.15 M NaCl, 0.015 M sodium phosphate, pH 7.4 (PBS) for three 5-min washes at room temperature. The vessel segments were bisected with iridectomy scissors; care was taken to preserve vascular wall structure. These parallel pieces from control and experimental carotid vessels were then treated with nonimmune or affinity-purified antibodies to actin and prepared for fluorescence microscopy as previously described (12, 14). Fluorescence from the experimental and control groups were recorded on Tri-X negative film (ASA 1000; Eastman Kodak, Rochester, NY) and developed in Acufine developer (Acufine Inc., Chicago, IL) (12).

Preparation of Canine Carotid Vessel Segments for Scanning Electron Microscopy. For scanning electron microscopy (SEM), vessel segments were refixed for 1.5 h at room temperature in a solution containing 2% formaldehyde and 3% glutaraldehyde DME buffered with 10 mM Hepes, pH 7.0. After refixation, the specimens were rinsed with PBS before submersion in 1% osmium tetroxide buffered with 0.1 M sodium phosphate, pH 6.0, for 30 min on ice. This step preceded a deionized H_2O rinse and an alcohol dehydration series beginning with 50% EtOH followed by steps in 70, 95, and 100% EtOH, each alcohol step lasting 20 min. Vessel segments were taken through the critical point in a Tousimis SAMDRI 790 before sputter coating in a Polaron SEM coater (Polaron Instruments, Inc., Hatfield, PA) operated at 0.6–0.625 kV for 0.5 min at 0.13 torr. Metal-coated specimens were observed at 9.0 kV in an ISI DS 130 scanning electron microscope. Negatives were exposed on Polaroid 55 film.

Quantification of Endothelial Cell Shape. To quantitate the EC shape as a function of hemodynamics, a number of parameters were calculated. While measurements of area and perimeter yielded statistically significant

Figure 6. Effects of altered transmural pressure and vessel compliance on endothelial cytoskeletal array (group II simulations). "Rigid" (*a, c,* and *e*) and "compliant" (*b, d,* and *f*) vessels were effectively created by altering the transmural pressure as described in Materials and Methods and in Brant et al. (2, 3). Pressure-perfused fixed carotids were then permeabilized and incubated with affinity-purified anti-actin antibodies labeled with rhodamine. Note that as a function of time (*a* and *b,* 3–4 h; *c* and *d,* 15 h; *e* and *f,* 23 h), the EC shape and cytoskeletal array are distinctively altered. (*a* and *b*) Early on spotted fluorescence in elongated cells is noted and this corresponds to EC microvillar expression in response to the flow dynamics (cf., Fig. 7 *a*). EC retraction follows the expression of microvilli (*c* and *d*) seen earlier as the cells have become spindlelike. (*c*) It appears that the antiactin staining is banded. This corresponds to the involutions in the plasmalemma (cf., Fig. 7 *b*). By 23 h the EC lining the rigid vessel (elevated TP group II vessels of Table II) have respread, developed extensive intercellular borders, and have assembled numerous stress fibers that are oriented with the long axes of the cells and are oriented with blood flow (*e*). (*f*) Lowering the transmural pressure has effectively elevated compliance vs. the "rigid vessels"; there are regions devoid of fluorescence and the cells do not show a preferential orientation to fluid flow. Additionally, no stress fibers are seen in these EC with diffuse fluorescence (×985). Bars, 10 μm.

294

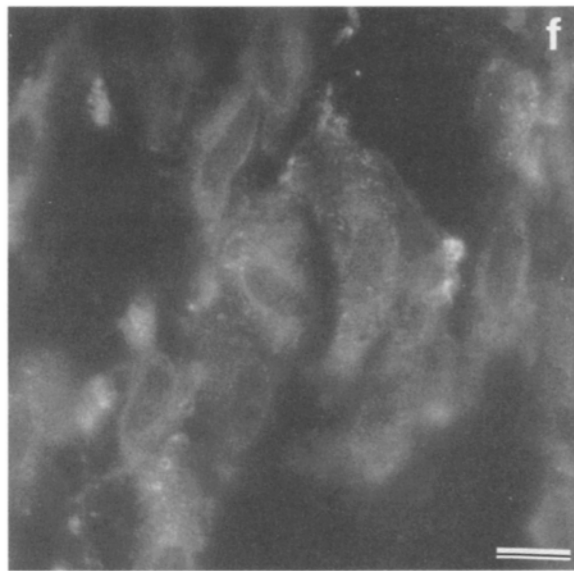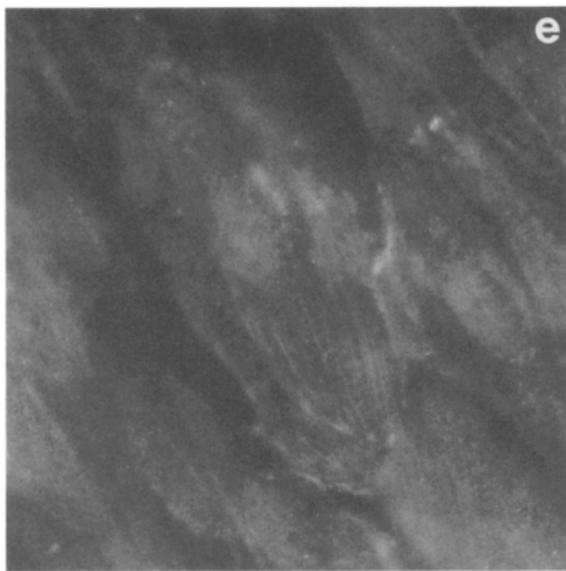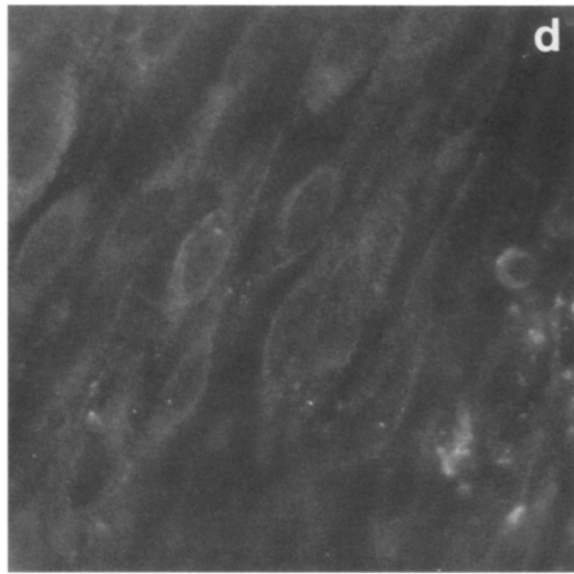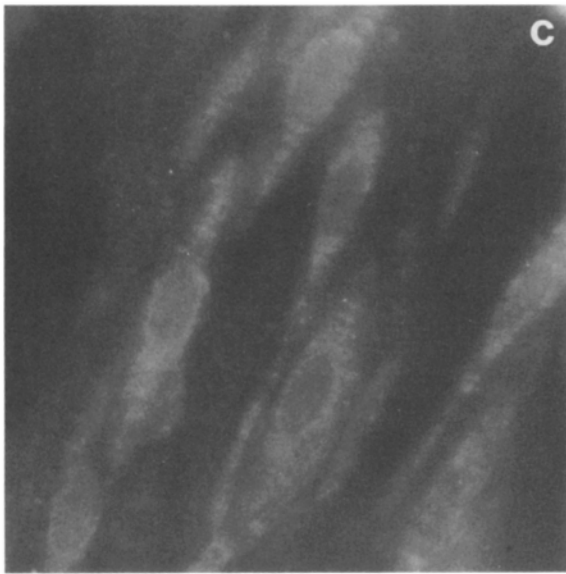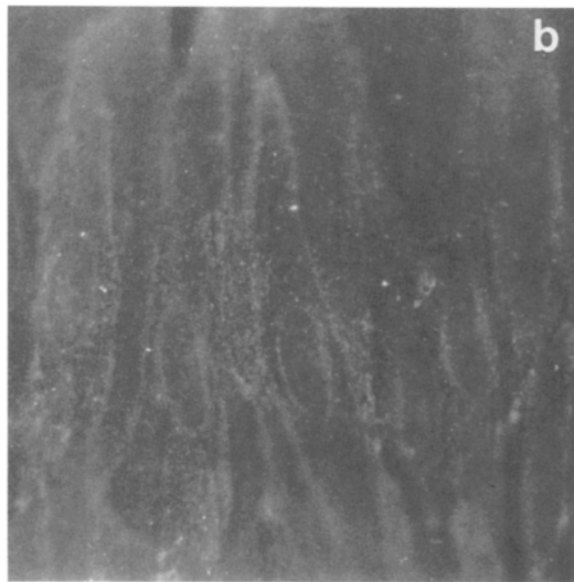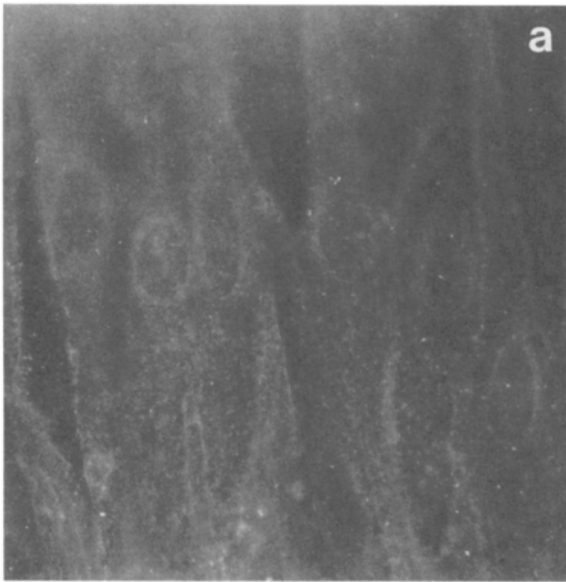Table II. Biologic Response of Carotid Vessels to Defined Hemodynamics

Group	Simulation	4-^{14}C carotid cholesterol uptake*	Shape index‡ (h)				Actin array§		
			0	3	15	24	D	C	SF
I	Normotension	8.1 (0.8)	0.20 (0.02)	−	−	0.20 (0.01)	+	−	−
II	Normotension −↑TP	32.5	0.19 (0.02)	0.11 (0.01)	0.17 (0.03)	0.65 (0.03)	+	−	10 (2)
II	Normotension −↓TP	20.3	0.19 (0.02)	0.12 (0.02)	0.17 (0.02)	0.54 (0.03)	+	+	−
III	↑PP/↑TP	11.3 (1.9)	0.23 (0.05)	−	0.16 (0.01)	0.27 (0.03)	+	−	−
III	↑PP/↑TP/↑flow	79.8	−	0.18 (0.04)	0.16 (0.02)	0.15 (0.03)	+	−	4 (1)
III	Hypertension/↑flow	−	−	0.15 (0.05)	−	0.18 (0.02)	−	+	−

Abbreviations: PP, pulse pressure; TP, transmural pressure.
* Normalized carotid blood vessel cholesterol uptake derived from the measured (liquid scintillation counting) radioactivity of [4-^{14}C]cholesterol. Data are expressed as the ratio of the [4-^{14}C]cholesterol content in the media compartment to that in the serum perfusate ($\times 10^3$). Values represent the mean from 25 representative experiments. Standard errors are in parentheses.
‡ Shape index was computed in a blind fashion by digitizing the width-to-length ratios of over 200 EC from each group and time point as described in the methods. Numbers are mean values with the standard errors in parentheses.
§ EC actin array was scored as predominantly diffuse (D), cortical (C), and/or with stress fibers (SF). Over 200 cells per group/time point were evaluated in a blind fashion as described in the methods. Numbers are mean SF/cell at 24 h of simulated flow with standard errors in parentheses.

data, the width-to-length axial ratio was equally informative in generating a significant database of EC shape. Ratio measurements involved sampling over 200 cells in each group of Table I in a blind fashion where the mean lengths and widths of the cells (together with the standard errors [SE]) were mapped through the centroid of cellular mass (which often corresponded to the nuclear region). Cells that were much longer than they were wide had a fractional axial ratio whereas cells that approximated a circle or those cells lacking an orientation to flow had an axial ratio that approached 1.0.

Quantification of Endothelial Stress Fibers. The number of EC stress fibers was quantitated in a blind fashion in over 200 cells from fluorescence micrographs of antibody-stained vessel segments exposed to the various hemodynamics of Table I. The mean stress fiber counts together with the standard error of the mean was then calculated for each hemodynamic condition.

Results

PDA and Intimal Integrity

We have carefully verified that the PDA reliably reproduced over 24 h each of the hemodynamic environments listed in Table I. For example, the mean transmural pressure measured in one representative experiment of ↑PP/↑TP/↑flow (group III of Table I) equaled 183 mmHg at 2 h, 187 mmHg at 10 h, and 173 mmHg at 20 h. The corresponding mean rates of flow were 295 ml/min (2 h), 296 ml/min (10 h), and 289 ml/min (20 h). Actual dynamic tracings of proximal perfusion pressure (P_1 of Fig. 3), flow rates (F_1), and arterial geometry obtained in one representative experiment are presented in Fig. 4. In addition to validating the reliability and accuracy of the pulsatile perfusion apparatus, we assessed our technique for tissue handling as it related to EC integrity. Here the exact protocol cited above for vessel excision, placement in the PDA, and removal for perfusion fixation was followed. Intimal integrity was maintained for these no-flow controls as well as for canine carotids perfused under normotensive control conditions (Fig. 5; group I in Table I). Contiguous, nonoverlapping EC were seen with their long axes oriented with perfusate flow (Fig. 5).
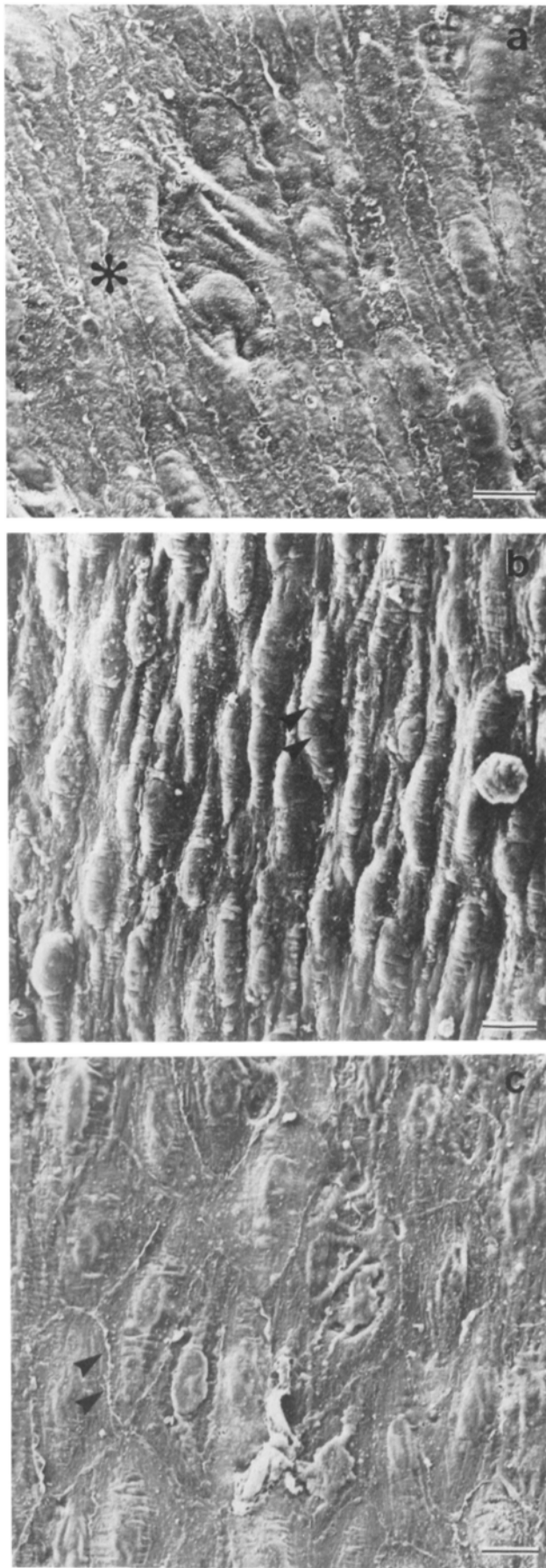
Carotid Cholesterol Uptake

To ascertain the effects of defined hemodynamics on the ability of the arterial intima either to restrict or permit passage of large macromolecules, we examined the incorporation of cholesterol as a function of defined flow phenomena. As is

shown in Table II, under normal flow and pressure conditions the ratio of labeled cholesterol present in the arterial media to that in the serum perfusate equaled 0.81%. In contrast, altering the motion of the vessel wall, by reducing or increasing the transmural pressure, potentiated the arterial accumulation of lipoprotein three- to fourfold. Interestingly, there was no significant difference between group I and group III (↑PP/↑TP). However, compounding the effects of elevated pulse and transmural pressures with increased flow caused ∼10-fold increase in cholesterol that accumulated in the media.

Hemodynamics, Endothelial Morphology, and Cytoskeletal Actin

Transmural Pressure Effects. We were interested in learning whether varying transmural pressure while maintaining flow rate and pulse pressure within physiologic ranges (group II vessels) influenced the EC adhesivity for their neighboring cells or extracellular matrix components via alterations in the cytoskeleton. Using the antibodies specific for actin, we could observe its dynamic response as a function of specific hemodynamic simulations (Figs. 6–11).

If the carotid vessels that were subjected to elevated or depressed transmural pressures for perfusion periods up to 2 h were pressure-fixed and then incubated in the affinity-purified antibodies to actin, no alterations in baseline morphology or cytoskeletal array were seen. At 2–2.5 h and for longer exposures to pulsatile flow, distinctive changes were observed. For example, the initial endothelial responses seen occurred when the cells expressed a spotted actin fluorescent pattern (Fig. 6, *a* and *b*). This was not seen in the normotension control cells stained with antiactin (cf., Fig. 10 *b*) nor the preimmune stained preparations which failed to stain the EC (data not shown). With the SEM, the spots were seemingly coincident with numerous microvilli that projected into the vessel lumen (Fig. 7 *a*, *asterisk*). These microvilli could not be seen projecting from the surface of the EC in the SEM images taken from the normotension controls (cf., Fig. 10 *a*). While the cells were contacting their neighbors at zero time, the EC retraction was obvious some 10–15 h later (Figs. 6, *c* and *d*; 7 *b*). This was not found for the control perfusion conditions (group I) in which no change in endothelial in-

tegrity was identified for as long as the experiments were conducted (up to 24 h; see e.g., Fig. 10 b). The most noticeable alteration occurring in association with endothelial retraction was an apparent banding of actin staining (Fig. 6, c and d). This banding was quite regular with bright and dark zones of relatively uniform thickness (Fig. 6 c). The diameters of the dark and light zones of banding seen in the fluorescence microscope corresponded in size to the folded and retracted regions of membrane circumscribing these EC and observed with SEM (Fig. 7 b, black arrowheads). Later, during these group II experiments effectively producing a decrease in vessel compliance (normotension-↑TP), the EC respread (Figs. 6 e; 7 c). These cells assembled several stress fibers oriented with perfusate flow (Table II). Stress fibers were seen in the respread cells, the apical surface area of which increased three- to fourfold during the 24 h of simulated flow (Figs. 6 e; 7 c).

On the other hand, group II vessels with enhanced arterial compliance (normotension-↓TP) displayed EC that completely lacked stress fibers at the 24-h time point (Fig. 6 f and Table II). Indeed, the cells had spread considerably between 2 and 24 h since the axial ratios (width-to-length) altered some threefold (Table II), indicating that the EC shape became more circular in nature. This was associated with a marked diffuse actin antibody staining which was highlighted in the cell periphery with bright, localization of what appeared as membrane ruffles and pseudopodia (Fig. 6 f). During both of these group II simulations of altered transmural pressure some loss of endothelial integrity occurred, especially if simulations were continued for 24 h. This could be detected in the fluorescence microscope as regions completely devoid of staining (Fig. 6 f). However, for the most part EC coverage was fairly complete.

Pulse Pressure Effects. Under the experimental conditions that simulated increased pulse and transmural pressures with normal flow (group III of Table I), the EC were found to be contiguous, elongated, and oriented with flow (cf., Table II). After 24 h of normal flow (150 ml/min) at PP = 120 mmHg, endothelial morphology and cytoskeletal array were virtually unchanged (Fig. 8). In some cases the axial ratio of the cells altered slightly (Table II), shifting to a more polygonal configuration, but this shift was not statistically significant. Additionally, 5% (1 in 20) of the cells displayed stress fibers (Fig. 8 c, *lower right*) but these cells were rare in all of the preparations examined under this hemodynamic condition.

Figure 7. SEM of canine carotid EC exposed to altered transmural pressure (group II simulations). "Rigid" vessels (normotension–↑TP) were created as described in Materials and Methods and presented after antiactin fluorescence in Fig. 6, *a, c,* and *e.* Note that the spotted fluorescence seen in Fig. 6 *a* corresponds to numerous microvilli projecting into the vessel lumen (lower left and upper right of *asterisk* in panel *a*). The fluorescent banding of Fig. 6 *b* can be accounted for by the wormlike appearance of the EC and the infoldings (*black arrowheads*) along the length of the now spindle-shaped cells whose centroids of mass (nuclear regions) are protruding into the vessel lumen. By 23 h, the cells have respread and have formed elaborate intercellular junctions (*c, black arrowheads*). (*a*) ×927; (*b*) ×838; (*c*) ×865. Bars, 10 μm.

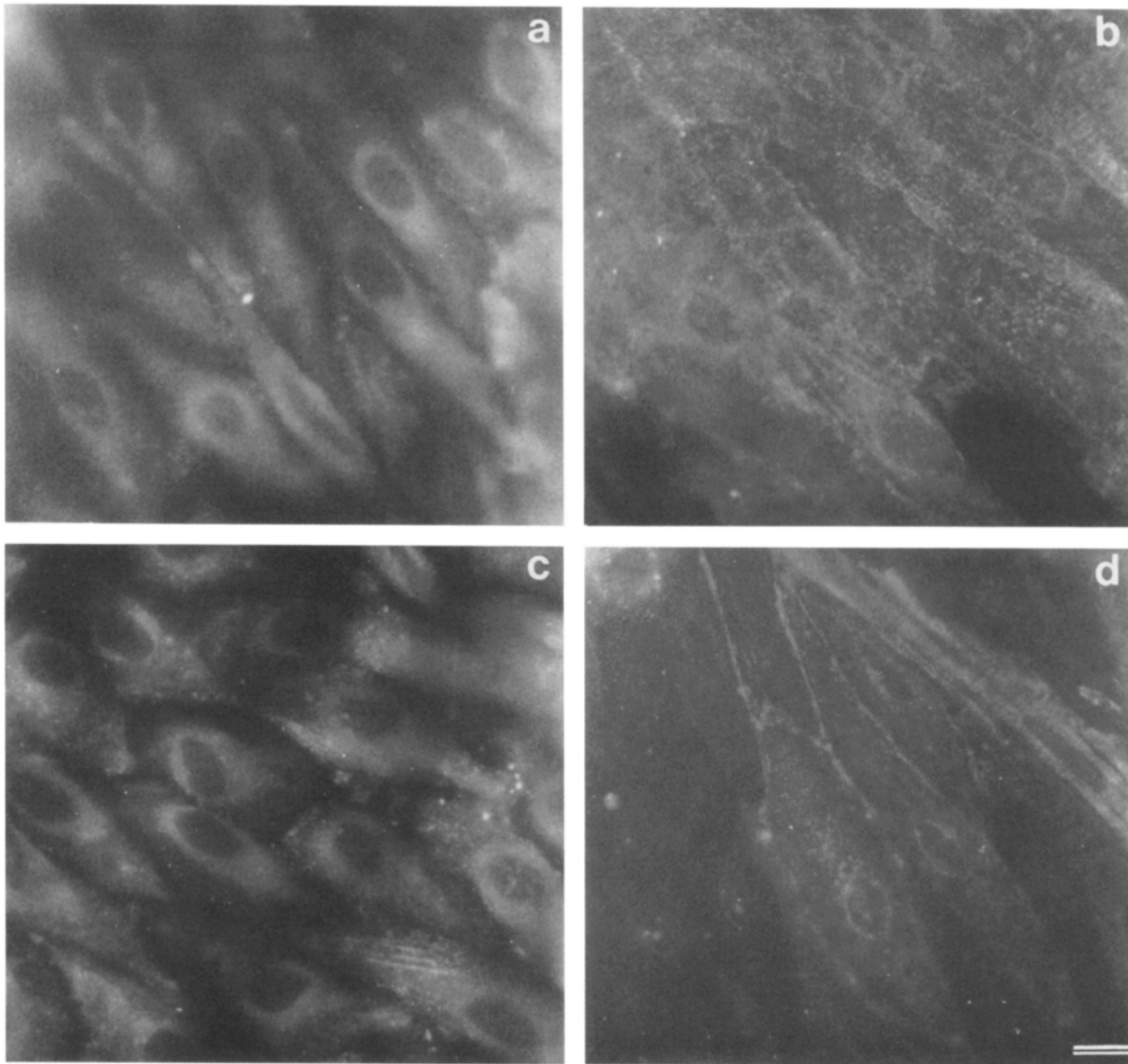*Figure 8.* Effects of intralumenal pressure and rate of flow on EC integrity and cytoskeletal array. (*a* and *c*) 240/120 mmHg, 150 ml/min (↑PP/↑TP); (*b* and *d*) 240/120 mmHg, 300 ml/min (↑PP/↑TP/↑flow). (*a* and *b*) 2.5 h; (*c* and *d*) 24 h. (*a–d*) Rhodamine antiactin staining. At normal flow conditions where the mean transmural pressure is 180 mmHg and the pulse pressure is 120 mmHg, there are no apparent alterations in the shape, orientation, or cytoskeletal arrays seen in the carotid EC. However, by 2.5 h under high flow, increased pulse and transmural pressures (*b*), the uniform amorphous antiactin fluorescence is replaced with a more spotted or reticulated staining pattern. After 24 h of this hemodynamic simulation, the EC have elongated, and much of the actin staining is missing except for the staining at the borders where the cells meet their neighbors and in association with the perinuclear region. The regions devoid of fluorescence (*d*, *left-hand side*) are not caused by EC loss since they can be seen with SEM (cf., Fig. 9 *d*) (×955). Bars, 10 μm.

Flow Effects. During the high flow (300 ml/min) simulations performed at PP = 120 mmHg, the vascular EC behaved in a distinctive manner. Spotted actin fluorescence was seen in the light microscope (Fig. 8 *b*) and numerous microvilli were seen via SEM projecting into the lumen of these same vessels (Fig. 9). Within the time course of the 24-h simulation, the axial ratio (Table II) was that of an elongated cell (0.15) and the apical surface area was computed to be two to three times that of the aforementioned EC in the normal flow vessels. Additionally, the only actin staining that persisted under these extreme hemodynamics was the perinuclear and cortical actin staining of the circumferential microfilamentous bundle (Fig. 8 *d*). Moreover, many EC

were devoid of actin staining (Fig. 8 *d*) despite the demonstration of EC presence by SEM (Fig. 9, *c* and *d*).

To determine whether the effects seen in Figs. 8, *b* and *d* would be ameliorated by reductions in pulse and transmural pressures, we subjected the canine carotid vessel segments to hypertensive flow dynamics. As seen in Fig. 10, the EC population is deficient of stress fibers under normotensive, group I conditions (Fig. 10 *b* and Table II). Contrarily, actin antibody staining and fluorescence microscopy revealed that the carotid EC of vessels perfused under hypertension/↑flow conditions (group III) assembled stress fibers after 15–24 h of flow (Fig. 10, *c* and *d* and Table II). Whereas the axial ratio of the cells was unchanged, the apical surface area nearly
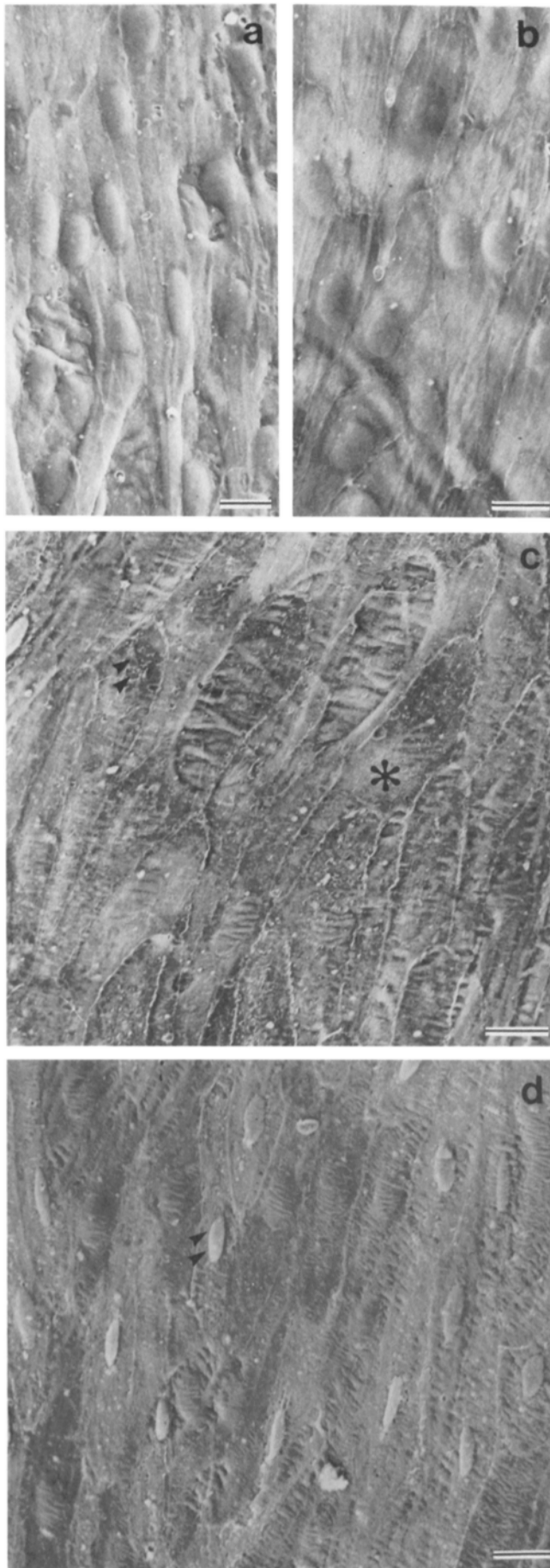
doubled when these high-flow experimentals were compared with normal flow, normotension (group I) cells. This rise in surface area of the former group was accompanied by what appeared to be a relative increase in actin staining under the control staining conditions, i.e., if identical antibody concentrations, reaction times, and incubation temperature were used for staining EC of the two groups. Stress fibers ($\overline{X}$ ~4/EC) that assembled along the abluminal cytoplasmic domain (as determined by through focusing) were oriented with flow (Fig. 10, c and d and Table II).

If we compared the endothelial cytoskeletal arrays from the hypertensive high-flow simulations with the ↑PP/↑TP/↑flow simulations, two facts became readily apparent. First, the axial ratios in each of the groups shifted somewhat as the cells elongated with flow (Fig. 11). Second, the cortical cytoskeleton responded uniquely when compared with the interior (or stress fiber) cytoskeleton, i.e., elevated flow in the absence of markedly elevated pulse and transmural pressures was sufficient to induce stress fiber assembly. Because insignificant stress fiber assembly was documented for the situation of ↑PP/↑TP (Fig. 8 c and Table II), we do not attribute the findings of Fig. 10, c and d to elevated pulse and transmural pressures alone. Finally, only the perinuclear and cortical cytoskeleton (where the EC meet their neighbors) were capable of withstanding the extreme hemodynamics of ↑PP/↑TP/↑flow.

Discussion

There is considerable evidence to suggest that hemodynamics play an important role in the pathogenesis of occlusive vascular disease (10, 18, 19, 23). However, because of the complexity of fluid flow within the vascular tree and the difficulty in studying individual hemodynamic parameters under controlled conditions in vivo, the exact mechanisms important in intimal destabilization are not well characterized (24). As a result, a number of investigators interested in this vascular disease process have turned their attention to the development of valid in vitro models to study the effects of arterial hemodynamics on the vascular wall cells. For example, alignment of vascular EC in a parallel plate and rotating cone viscometer has been observed as has the alignment of the stress fiber-rich cytoskeleton (7–9). However, in all

Figure 9. SEM of carotid EC subjected to increased flow, pulse and transmural pressures (↑PP/↑TP/↑flow). (a and b) 0 h; (c) 2.5 h; (d) 20 h. In panels a and b note the contiguous nature of the carotid EC in the zero time, surgery control specimens. The luminal EC surface is smooth, virtually devoid of microvilli, the cells are elongated, and the nuclei are uniformly ovoid in shape. As seen with fluorescence microscopy after staining with antiactin antibodies, 2.5 h later, the EC have developed numerous microvilli (c, to the immediate right of the *black arrowheads*) and the cell borders have become pronounced (below *asterisk, c*). In panel d, after 24 h of this simulation, the endothelial nuclei have taken on a more heterogeneous shape distribution with the majority appearing quite elongated with pointed ends (*arrowheads*). In this and other specimens exposed to this hemodynamic situation, the EC have a darkened appearance (group of three cells just to the right of the cell pointed at by the *black arrowheads*). These darkened cells seen in the scanning microscope could represent the regions devoid of fluorescence seen in Fig. 8 d. (a) ×721; (b) ×855; (c) ×923; (d) ×877. Bars, 10 μm.
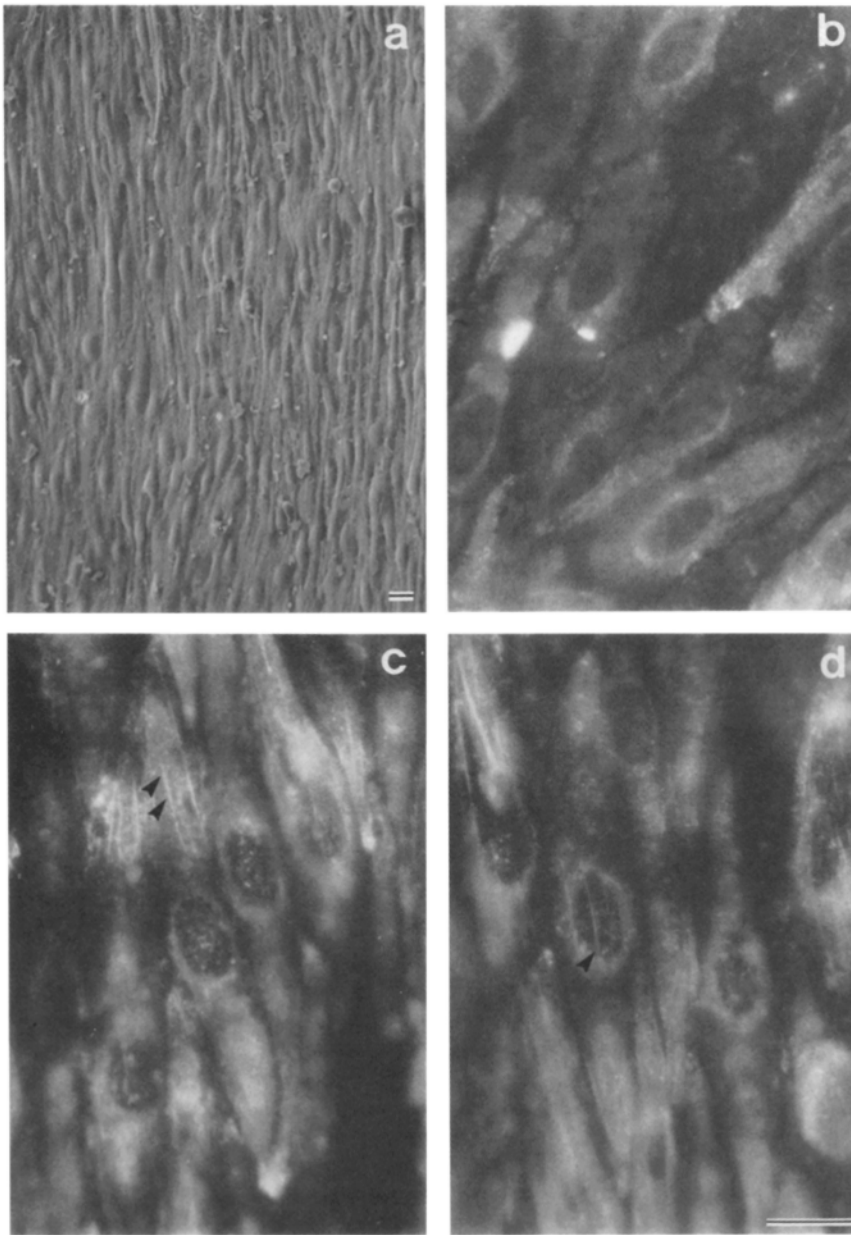
Figure 10. Effects of elevated flow rate (hypertension/↑flow) on carotid EC actin organization. Carotid blood vessel segments were subjected to increased flow rates in the absence of extreme elevations in the pulse and transmural pressures. In panel *a* a low-power SEM of the group I control is shown with contiguous EC oriented with blood flow. A corresponding antiactin-stained specimen is shown for this specimen at higher power in panel *b*. Note that in panel *b*, there are no signs of stress fibers present but that in the two random fields from two separate experiments, the EC subjected to 270 ml/min flow for 24 h have assembled stress fibers oriented with fluid flow (*black arrowheads* in panels *c* and *d*). (*a*) ×293; (*b–d*) ×1,024. Bars, 10 μm.

such sets of pioneer bioengineering studies, EC were placed on a rigid glass or plastic substrate. Recent work in our laboratory and by others indicates that the substrate significantly influences vascular EC behavior, including, e.g., the migratory response to injury (29).

Using the pulse duplicator of Fig. 2 to model the cardiac cycle in an explanted artery, we were able to alter hemodynamics in a "one step at a time fashion" (1–3). After staining for endothelial cytoskeletal actin, it became increasingly clear that (*a*) rate of flow, more so than transmural and pulse pressure, initially influenced an EC cytoskeletal array (group III vessels); and (*b*) variations in transmural pressure and vessel wall compliance maintained with normal rates of flow and pulse pressures (group II vessels) also caused EC cytoskeletal rearrangements (Table II). Whereas other groups have studied the effects of steady flow upon EC function and morphology, the present work marks, to the best of our

knowledge, an initial effort to predict the combined effects of pulsatile pressure and flow phenomena.

One of the most interesting findings of these interdisciplinary studies was that the cortical endothelial cytoskeleton responds differently to pressure and flow phenomena than does the stress fiber cytoskeleton. The dense, peripheral band or the circumferential, microfilamentous network of actin filaments has been implicated in vascular endothelial integrity. Wong and Gotlieb (27) suggest that the dense, peripheral band is an organelle mediating the response to single-cell injury in vitro; i.e., the disassembly of the cortical cytoskeleton occurs as the EC bordering the wound site spread out to restore confluence. Our results indicate that the band of microfilamentous actin surrounding the nucleus and bordering the plasma membrane resists disassembly under extremes of hemodynamic stress; i.e., TP = 240/120 mmHg, PP = 120 mmHg, and flow rate = 300 ml/min. In
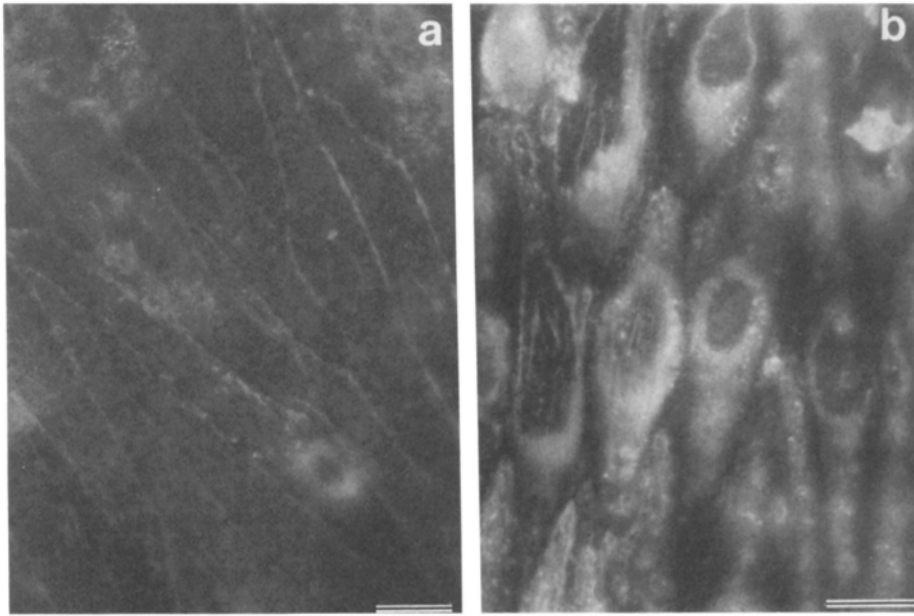
Figure 11. Comparison of the anti-actin-stained EC lining the carotid blood vessels subjected to (*a*) increased pulse and fluid pressures and elevated flow rates (↑PP/↑TP/↑flow) and (*b*) hypertensive hemodynamics. Note that the actin staining in panel *a* is restricted to the cell cortices and the perinuclear region whereas the EC in panel *b* subjected to the same flow rates but without the marked elevations in pulse and transmural pressure have stress fibers and a robust actin staining throughout the cytoplasm. Perfusion time, 24 hours. (*a*) ×955; (*b*) ×1,024. Bars, 10 μm.

so doing, endothelial–endothelial as well as endothelial–basal lamina interactions must certainly be facilitated so that endothelial integrity is maintained. Thus, under our experimental conditions, which model extreme pathologic hemodynamics in vivo, only the cortical endothelial actin cytoskeleton seemingly remains intact.

It is interesting to consider the reasons why the simulation of ↑PP/↑TP failed to influence significantly either macromolecular transport or endothelial morphology and cytoskeletal array (during the time course studied), whereas the simulation of normotension-↑TP produced marked alterations in cell shape, EC actin array, and cholesterol uptake (Table II). As seen in Table I, both studies were conducted at the same physiologic flow rate (150 ml/min) and TP (170–180 mmHg). The only apparent difference is that the group III simulation imposed a pulse pressure of 120 mmHg on the test vessels vs. 40 mmHg for the case of normotension-↑TP. Intuitively, one might expect that elevated pulse pressure itself could produce deleterious effects upon the delicate EC; yet, the opposite finding was documented. One possible explanation might be the difference in vessel wall geometry during pulsatile perfusion for these two simulations. For example, because of the elevated pulse pressure, the change in internal vessel radius or vessel wall thickness (Fig. 4) measured during the simulation of ↑PP/↑TP (7.1%) significantly exceeded that (2.7%) when normotension-↑TP conditions were imposed upon the test vessels (2, 3). At the microscopic level, the increased motion of the vessel wall associated with these group III experiments may have "anchored" the EC to the underlying substratum as indicated by the EC shifting to a more polygonal shape (Fig. 8) and the presence of EC stress fibers observed for the normotension-↑TP simulations (Fig. 6).

Another interesting result of this work is that simultaneous elevations in pulse and transmural pressures (normal flow) fail to alter EC morphology or the cytoskeletal array of actin. In contrast, elevations in flow rates from 150 to 270 ml/min were sufficient to induce stress fiber assembly in the direc-

tion of fluid flow (Table II). Increased surface area was also seen under these conditions as well as during the simulations producing less compliant carotid vessels (normotension-↑TP). In each of these simulations, i.e., during the elevated flow and group II experiments, stress fiber assembly occurred along the abluminal plasma membrane. Early work in our laboratory and by others has put forth a role for stress fibers in promoting the adhesion of cells to the underlying substrate, by virtue of the attachment of actin filament bundles to the membrane. This complex, in turn, is associated with the components of the basement membrane's extracellular matrix. In fact, molecules of the basement membrane (e.g., pepsin fragments of type IV collagen, fibronectin, and an endothelial-derived pericellular coat consisting of laminin, fibronectin, proteoglycan, and collagens) have been documented to induce stress fiber assembly in aortic EC recovering from injury in vitro (29), thereby retarding the migration associated with injury. There is also one preliminary study suggesting that the actin-associated proteins believed to participate in tethering the cytoskeleton to the plasma membrane are also influenced by the composition of the extracellular compartment (22).

Not only may the composition of the extracellular matrix be important in signaling EC cytoskeletal array, but vessel deformability may play a significant role in the regulation of intimal integrity. Comparisons of EC morphology from group II experiments suggest that the EC response to increased or decreased vessel compliance may be similar. In actuality, antiactin staining indicates that this is not the case (Fig. 6). Each of these simulations causes EC retraction. This is followed by EC spreading, which leads to an increased shape index, reflected as a decreased alignment with blood flow. Based upon the shape index and antibody localization data, we predict that increased compliance would potentiate EC migration, seen as the diffuse antiactin staining pattern. Stimulation of EC migration might occur secondarily to the loss of EC contact when neighboring cells are displaced. On the other hand, the simulation of a "rigid"

blood vessel (by increasing the transmural pressure) elevates the circumferential stresses acting on the vessel wall (3). This, in turn, may be the cause of EC stress fiber assembly over the same experimental time course, reflecting a need for enhanced adhesion.

Our results also suggest that the induction of carotid EC stress fibers accompany local elevations in the flow velocity. Similar rises in velocity are seen secondarily in association with arterial stenoses, suggesting that an effective narrowing of luminal radii accompanying vascular pathophysiology may cause similar EC behavior in vivo. Perhaps under conditions of prolonged elevated pressure and flow velocities, EC stress fiber disassembly would leave only the circumferential microfilaments and those actin filaments that apparently encircle the nucleus intact. If these endothelial adaptive hemodynamic responses are site specific, this may help explain the characteristically focal nature of atherogenesis.

Fry (10), Caro and Nerem (5), and Chien et al. (6) have studied the effect of hemodynamic/biomechanical factors (e.g., shear stress, stretch, and vibration) on the transport of macromolecules into the arterial wall. It has generally been shown that enhanced uptake is associated with mechanical disturbances. The present findings of Table II complement these earlier investigations in that all experiments were performed on arterial tissue exposed to realistic pulsatile pressure and flow phenomena. For the measurements made of vessels ($n = 10$) exposed to group I control hemodynamics, our predictions of arterial wall uptake compare favorably with in vivo data obtained for the rabbit thoracic aorta by Bratzler et al. (4) and Ramirez et al. (23). A different picture emerges for the group II and group III perfusion experiments; that is, the magnitude of cholesterol uptake rises above that documented for the group I controls and appears to be correlated with alterations in EC shape and cytoskeletal array. Such correlations between arterial wall uptake and intimal integrity are consistent with theoretical calculations recently performed by Nir and Pfeffer (21). They demonstrated that with as little as 3% of the endothelial surface damaged with locally spread holes of size equal to 10% of the thickness of the arterial media, macromolecular transport can increase by a factor of 2.5 over that for an artery with no endothelial damage. This suggests that alterations in EC shape and actin array might be associated with the elevated uptake of lipoprotein molecules observed in vivo. Clearly, these and other factors must be more carefully examined before hemodynamics-induced arterial injury is understood.

References

1. Brant, A. M., J. F. Chmielewski, T.-K. Hung, and H. S. Borovetz. 1986. Simulation *in vitro* of pulsatile vascular hemodynamics using a CAD/CAM designed cam disc and roller follower. *Artif. Organs (Cleve.).* 10:419–421.
2. Brant, A. M., V. G. J. Rodgers, and H. S. Borovetz. 1987. Measurement in vitro of pulsatile arterial diameter using a helium-neon laser. *J. Appl. Physiol.* 62:679–683.
3. Brant, A. M., S. S. Shah, V. G. J. Rodgers, J. Hoffmeister, M. F. Teodori, I. M. Herman, R. L. Kormos, and H. S. Borovetz. 1987. Biomechanics of the arterial wall under simulated flow conditions. *J. Biomech.* In press.
4. Bratzler, R. L., G. M. Chisolm, C. K. Colton, K. A. Smith, D. B. Zilversmit, and R. S. Lees. 1977. The distribution of labelled albumin across the rabbit thoracic aorta in vivo. *Circ. Res.* 40:182–190.
5. Caro, C. G., and R. M. Nerem. 1973. Transport of ¹⁴C-4 cholesterol between serum and wall in the perfused dog common carotid artery. *Circ. Res.* 32:187–205.
6. Chien, S., M. M. L. Lee, L. S. Laufer, D. A. Handley, S. Weinbaum, C. G. Caro, and S. Usami. 1981. Effects of oscillatory mechanical disturbance on macromolecular uptake by arterial wall. *Arteriosclerosis.* 1:326–336.
7. Dewey, C. F., S. R. Bussolari, M. A. Gimbrone, Jr., and P. F. Davies. 1981. The dynamic response of vascular endothelial cells to fluid shear stress. *J. Biomech. Eng.* 103:173–85.
8. Frangos, J. A., S. G. Eskin, L. V. McIntire, and C. L. Ives. 1985. Flow effects on prostacyclin production by cultured human endothelial cells. *Science (Wash. DC).* 277:1477–1479.
9. Franke, W. W., M. Grafe, H. Schnittler, C. Mitermayer, and D. Drenckhahn. 1984. Induction of human vascular endothelial stress fibers by fluid shear stress. *Nature (Lond.).* 307:648–49.
10. Fry, D. L. 1968. Acute vascular endothelial changes associated with increased blood velocity gradients. *Circ. Res.* 22:165–67.
11. Gabbiani, G., F. Gabbiani, D. Lombardi, and S. M. Schwartz. 1983. Organization of the actin cytoskeleton in normal and regenerating arterial endothelial cells. *Proc. Natl. Acad. Sci. USA.* 80:2361–64.
12. Herman, I. M., N. J. Crisona, and T. D. Pollard. 1981. Relation between cell activity and the distribution of cytoplasmic actin and myosin. *J. Cell Biol.* 88:84–91.
13. Herman, I. M., and P. A. D'Amore. 1984. Capillary endothelial migration: loss of stress fibers in response to retina-derived growth factor. *J. Muscle Res. Cell Motil.* 5:631–640.
14. Herman, I. M., T. D. Pollard, and A. J. Wong. 1982. Contractile proteins in endothelial cells. *Ann. N.Y. Acad. Sci.* 401:50–60.
15. Lautsch, E. V., G. C. McMillan, and G. L. Duff. 1953. Techniques for the study of normal and atherosclerotic arterial intima from its endothelial surface. *Lab. Invest.* 2:397–407.
16. Lewis, W. H., and M. K. Lewis. 1924. Behavior of cells in tissue culture. *In.* General Cytology. E. V. Cowdry, editor. University of Chicago Press, Chicago, IL. 385–447.
17. Lewis, L., H. M. Yerna, S. S. Levinstone, L. Marek, and E. Bell. 1982. The relationship of fibroblast translocations to cell morphology and stress fiber density. *J. Cell Sci.* 53:21–37.
18. Masuda, H., Y. Kikuchi, T. Nemoto, A. Bukhari, T. Toyawea, and A. Kmiya. 1982. Ultrastructural changes in the endothelial surface of the canine carotid artery induced by wall shear stress load. *Biorheology.* 19:197–208.
19. Meyer, W. 1979. Hemodynamic contribution to atherosclerosis. *Adv. Exp. Med. Biol.* 115:353–466.
20. Newman, H. A. I., and D. B. Zilversmit. 1966. Uptake and release of cholesterol by rabbit atheromatous lesions. *Circ. Res.* 18:293–302.
21. Nir, A., and R. Pfeffer. 1979. Transport of macromolecules across arterial wall in the presence of local endothelial injury. *J. Theor. Biol.* 81:685–711.
22. Pratt, B. M., A. S. Harris, J. S. Morrow, and J. A. Madri. 1984. Mechanisms of cytoskeletal regulation: modulation of aortic endothelial cell spectrin by the extracellular matrix. *Am. J. Pathol.* 117:349–54.
23. Ramirez, C. A., C. K. Colton, K. A. Smith, M. B. Stemerman, and R. S. Lees. 1984. Transport of ¹²⁵I-albumin across normal and de-endothelialized rabbit thoracic aorta in vivo. *Atherosclerosis.* 4:283–91.
24. Ross, R. 1986. The pathogenesis of atherosclerosis. *N. Engl. J. Med.* 314:488–500.
25. Wang, Y. L. 1984. Reorganization of actin filament bundles in living fibroblasts. *J. Can. Biol.* 99:1478–85.
26. White, G. E., M. A. Gimbrone, Jr., and K. Fujiwara. 1983. Factors influencing the expression of stress fibers in vascular endothelial cells in situ. *J. Cell Biol.* 97:416–24.
27. Wong, M. K. K., and A. I. Gotlieb. 1984. In vitro re-endothelialization of a single cell wound: role of microfilament bundles in rapid lamellipodia-mediated wound closure. *Lab. Invest.* 51:75–81.
28. Wong, A. J., T. D. Pollard, and I. M. Herman. 1983. Actin filament stress fibers in vascular endothelial cells in vivo. *Science (Wash. DC).* 219:867–69.
29. Young, W. C., and I. M. Herman. 1985. Extracellular matrix modulation of endothelial cell shape and motility following injury in vitro. *J. Cell. Sci.* 73:19–28.